Two Novel Esterases from Deep-Sea Sediment Reveal Key Residues for Thermostability

Yi Ding
Shanghai Jiao Tong University
Xiao-chen Yang
Second Institute of Oceanography Ministry of Natural Resources
Ying-yi Huo
Zhejiang University
Shu-ling Jian
Second Institute of Oceanography Ministry of Natural Resources
Xue-we Xu
Second Institute of Oceanography Ministry of Natural Resources
Heng-lin Cui (cuihenglin@ujs.edu.cn)
Jiangsu University
Yue-hong Wu
Second Institute of Oceanography Ministry of Natural Resources https://orcid.org/0000-0002-1593-8662

Research Article

Keywords: deep-sea sediment, metagenomic library, family IV esterases, thermostability

Posted Date: April 26th, 2021

DOI: https://doi.org/10.21203/rs.3.rs-439445/v1

Abstract

Thermostability is one of the major concerns in the industrial application of enzymes. In this study, two novel family IV esterases, Est2 and Est4, were identified from a deep-sea sediment metagenomic library. The two enzymes had high amino acid sequence identity (96%) with only twelve different residues. Characteristic analysis indicated that both enzymes shared most of the enzymatic properties, including optimum *p*-nitrophenyl substrates (*p*-nitrophenyl butyrate and hexanoate), temperature (40°C) and pH (7.0–8.0). Interestingly, Est2 showed higher thermostability at 50°C than Est4. Mutagenesis analysis of Est2 identified two out of twelve differential amino acids, Asp18 and Lys289, that were crucial for the thermostability of the enzymes. Asp18 determined both the thermostability and catalytic activity of Est2. Structural analysis showed that Asp18 was located at the cap domain of Est2 and might be involved in the mobility of the cap domain. Lys289, located at the surface of Est2, determined the discrepancy in the surface potential between the two enzymes. Our results provide inspiration for research on the thermostability of esterases and improve the application potential of deep sea-derived esterases in industrial production.

1 Introduction

The marine environment is one of the largest pools of novel enzymes that could provide potential profits in many industrial fields. Metagenomics screening has become an efficient method for exploring novel enzymes from environments(Rappe and Giovannoni 2003). Currently, a large number of novel esterases, such as DMWf18-543, DMWf18-558(Huo et al. 2018), EstEP16(Zhu et al. 2013), and alkaline esterase EM2L8(Park et al. 2007), have been isolated from marine environments by metagenomic methods.

Esterase (EC 3.1.1.1), belonging to lipolytic enzymes, is a group of hydrolases that catalyze the cleavage and formation of short-chain acylglycerols(Arpigny and Jaeger 1999; Bornscheuer 2002). With broad substrate specificity, high stereospecificity and cofactor-independent catalytic mechanisms, esterases are of great significance in industrial applications(Jaeger and Eggert 2002). Lipolytic enzymes were classified into eighteen families based on their amino acid sequences and biological properties(Samoylova et al. 2018). The family IV esterases show the classical α/β hydrolase fold containing two distinct structural domains: catalytic domain and cap domain(Ollis et al. 1992). The Ser-His-Asp/Glu catalytic triad located on the catalytic domain is responsible for ester bond hydrolysis(Li et al. 2015). The conserved HGG motif of family IV esterases is involved in the formation of oxyanion holes and plays a key role in stabilizing the tetrahedral intermediate of the reaction(Mandrich et al. 2008). The cap domain located on the entrance of the catalytic pocket impacts the maintenance of enzyme stability, activity and specificity(Mandrich et al. 2005).

In this study, we described the expression, purification and biochemical characterization of two novel esterases, Est2 and Est4, that were screened from a deep-sea sediment metagenomic library(Jiang et al. 2012). The two enzymes had high amino acid sequence identity. Mutagenesis analysis identified two residues in Est2, Asp18 and Lys289, which had significant impacts on the catalytic features of the

enzyme. The Asp18Asn mutation of Est2 significantly affected the thermostability and catalytic activity of the enzyme. The residue Lys289 was identified as the key residue to determine the discrepancy of surface potential and thermostability between Est2 and Est4.

2 Materials And Methods

2.1 Sequence and polygenetic analysis

Two putative esterase genes with high amino acid sequence identity, designated *est2* and *est4*, were previously obtained from a deep-sea sediment metagenomics library using the subcloning method (Jiang et al. 2012). The deep-sea sediments were collected from the skirt of a seamount located in the Pacific Ocean at a depth of 5 886 m. Their deduced amino acid sequences were analyzed by the BLASTp program (https://blast.ncbi.nlm.nih.gov). Sequence alignment of the amino acid sequences of multiple proteins was performed using Clustal X version 2.0(Larkin et al. 2007) and ESPript 3.0(Robert and Gouet 2014). The corresponding phylogenetic tree was constructed using the neighbor-joining method with MEGA version 7.0 software(Kumar et al. 2016).

2.2 Homology modeling and putative structure analysis

The three-dimensional (3D) structures of Est2 and Est4 were modeled using the I-TASSER server (https://zhanglab.ccmb.med.umich.edu)(Roy et al. 2010). Structural figures were generated using PyMOL software (http://pymol.sourceforge.net).

2.3 Cloning, expression and purification

The *est2* and *est4* genes were amplified by polymerase chain reaction using the primers listed in **Table 1**. The PCR products were digested by *Nde*I and *Hin*dIII (New England BioLabs, USA). The purified digested fragments were ligated into the pET28b(+) (Novagen, Germany) expression vector that had been digested with the same enzymes. The recombinant plasmids were transformed into *Escherichia coli* (*E. coli*) Rosetta (DE3) cells.

Recombinant *E. coli* Rosetta (DE3) strains were cultivated in LB medium containing 50 μg/mL kanamycin and 34 μg/mL chloramphenicol at 37°C until the OD_{600} reached 0.8. Protein expression was induced by 0.5 mM isopropyl-β-D-thiogalactopyranoside (IPTG) for 20 h at 16°C. The cells were harvested by centrifugation at 4°C and 10 000 ×*g*, and were resuspended in 10 mM imidazole buffer containing 500 mM NaCl and 20 mM Tris/HCl (pH 8.0) for sonication. Protein samples were collected from the supernatant of cell lysates by centrifugation at 4°C and 18 000 ×*g* and were purified by Ni-NTA affinity chromatography columns.

2.4 Mutagenesis

The point mutants Est2-Asp18Asn (Est2-D18N) and Est2-Lys289Glu (Est2-K289E) were constructed by site-directed mutagenesis using wild-type recombinant plasmid as the template with the Fast Mutagenesis System (Transgene Biotech, China) via whole-plasmid PCR in 20 reaction cycles of 94°C for 20 s, 55°C for 20 s and 72°C for 3 min. The primers used for PCR are listed in **Table 1**. The verified mutant recombinant plasmids were transferred into competent *E. coli* Rosetta (DE3) cells for expression.

2.5 Enzyme activity assay

Enzyme activity was evaluated by measuring the UV absorption at 405 nm of *p*-nitrophenol at 40°C for 2 min with a DU800 ultraviolet–visible spectrophotometer (Beckman, USA). The 1 mL standard reaction mixture contained 10 μL of 100 mM *p*-nitrophenyl (*p*-NP) hexanoate, 980 μL of phosphate buffer (100 mM, pH 7.0), and 10 μL of the purified enzyme. All values were determined in triplicate, and reactions with the added thermally inactivated enzyme were used as controls. One unit of enzyme activity was defined as the amount of esterase required to release 1 μmol of *p*-NP per minute from the *p*-NP ester.

2.6 Enzyme characterization assay

The substrate specificity of the enzymes was determined using *p*-NP esters (Sigma, unless otherwise stated) as the substrates, including *p*-NP acetate (C2), *p*-NP butyrate (C4), *p*-NP hexanoate (C6) (TCI, Japan), *p*-NP octanoate (C8), *p*-NP decanoate (C10), *p*-NP laurate (C12), *p*-NP myristate (C14) and *p*-nitrophenyl palmitate (C16). The kinetic parameters were obtained by measuring the initial reaction rates of hydrolysis of *p*-NP butyrate (C4) and *p*-NP hexanoate (C6) at various concentrations ranging from 0.1 to 2.0 mM. GraphPad Prism 7.0 software (GraphPad Inc., USA) was used to calculate the kinetic parameters of the enzymes by analyzing the slopes of the Michaelis–Menten equations.

The optimum pH for enzyme activity was measured over a pH range from 3.0 to 10.0 with four different buffers, including 100 mM citrate buffer (pH 3.0–6.0), 100 mM phosphate buffer (pH 6.0–7.5), 100 mM tricine buffer (pH 7.5–9.0), and 50 mM CHES buffer (pH 9.0–10.0). The reactions at different pH values were measured at 348 nm, the pH-independent isosbestic wavelength of *p*-nitrophenol and *p*-nitrophenolate. The optimum temperature for enzyme activity was measured over a range of 15–60°C with an interval of 5°C. The thermostability of Est2 and Est4 was analyzed by measuring the residual activity after incubating the enzymes at different temperatures (ranging from 30°C to 60°C) in 100 mM phosphate buffer (pH 7.0) for 1 h.

The effects of various metal ions (Ba^{2+}, Ca^{2+}, Co^{2+}, Cu^{2+}, Mg^{2+}, Mn^{2+}, Ni^{2+}, Sr^{2+}, and Zn^{2+}) and the chelating agent ethylenediaminetetraacetic acid (EDTA) were examined at a final concentration of 10 mM. The effects of various detergents were determined using 1% (v/v) Triton X-100, Tween-20, Tween-80, and 1% (w/v) SDS. The effects of various organic solvents were examined using acetone, acetonitrile,

ethanol, N, N-dimethylformamide (DMF), dimethyl sulfoxide (DMSO), glycerol, isopropanol, and methanol at a final concentration of 15% (v/v). All tests were performed in 100 mM Tris/HCl buffer (pH 7.5), and the values obtained without additives in the reaction mixture were defined as 100%. Data were presented as the mean ± SD. Statistical analyses were performed with two-tailed unpaired Student's t-tests. P values less than 0.05 were considered statistically significant.

2.7 Nucleotide sequence accession numbers

The locus tags of the e*st2* and *est4* genes are JF766282 and JF766284, respectively.

3 Results

3.1 Sequence analysis of Est2 and Est4

The sequences of *est2* and *est4* were both 921 bp and encoded 306 amino acids with 96% sequence identity. The identified esterases in the GenBank nr database that shared the highest amino acid sequence identity (77-78%) with Est2 and Est4 were three metagenome-derived esterases, namely, FLS10, FLS15 and ScsEst01, obtained from South China Sea sediment(Hu et al. 2010; Zhang et al. 2015), followed by the esterases identified from soil and marine sediment metagenomes (**Table 2**).

Multiple sequence alignment showed that Ser144, Glu238, and His268 formed the catalytic triad of Est2 and Est4 (**Fig. 1**). The catalytic Ser144 is located in the conserved GDSAG motif (positions 142-146). Polygenetic analysis validated that Est2 and Est4 are new members of microbial esterases in family IV (**Fig. 2**).

3.2 Expression and characterization of wild-type Est2 and Est4

Est2 and Est4, with molecular weights of 32.5 kDa, were successfully expressed in *E. coli* Rosetta (DE3) and purified using Ni-NTA affinity chromatography columns. Est2 and Est4 had higher activities toward relatively short-chain *p*-NP esters (< C10) with the highest activity toward *p*-NP hexanoate than those with long-chain *p*-NP esters (≥ C10) (**Fig. 3a**). The catalytic activity of the two enzymes can be retained under a wide range of temperatures from 15°C to 45°C (**Fig. 3b**) and pH values from 6.0 to 8.5 (**Fig. 3c**). Both Est2 and Est4 exhibited the highest activity at pH 7.0-8.0 and 40°C.

Thermostability analysis showed that Est2 and Est4 maintained approximately 80% and 70% of their initial activities, respectively, after incubation at 40°C for one hour (**Fig. 3d**). Est4 completely lost catalytic activity, while Est2 retained 30% of its initial activity after incubation at 50°C for one hour.

The kinetic parameters of purified Est2 and Est4 were determined by using *p*-NP butyrate and *p*-NP hexanoate as substrates (**Table 3**). When *p*-NP hexanoate was used as a substrate, the *V*max and K_m of Est2 were (652.0±5.3) μmol·mg^{-1}min^{-1} and (55.0±3.0) μM, respectively, and those of Est4 were (605.6±5.9) μmol·mg^{-1}min^{-1} and (55.0±3.2) μM, respectively. When *p*-NP butyrate was used as a substrate, the *V*max and K_m of Est2 were (791.5 ± 18.7) μmol·mg^{-1}min^{-1} and (386.3± 24.6) μM, respectively, and those of Est4 were (620.2±16.4) μmol·mg^{-1}min^{-1} and (356.9±26.4) μM, respectively.

Est2 and Est4 showed high resistance to Ba^{2+}, Mg^{2+}, Sr^{2+} and Co^{2+} (more than 70% of their initial activities remained) but were markedly inhibited by Cu^{2+}, Mn^{2+}, Ni^{2+} and Zn^{2+} (**Table 4**). Est4 showed higher tolerance to all tested solvents, except glycerin, at 15% (v/v) than Est2 (**Table 5**). The addition of 1.0% SDS inactivated Est2 and Est4, while 1.0% Tween 20 enhanced Est2 activity but decreased Est4 activity (**Table 5**).

3.3 Structural model analysis

The 3D structures of Est2 and Est4 were modeled using the I-TASSER server. The protein structures of both enzymes contain 8 b-sheets and 9 a-helices. The structures could be divided into two domains: a catalytic domain (residues 45-305) with a canonical α/β-hydrolase fold consisting of eight parallel β strands surrounded by five α helices and a cap domain (residues 1-44) (**Fig. 4**). The global structures of Est2 and Est4 did not exhibit significant differences, while Est4 contained more negative surface potentials than Est2 (**Fig. 5**).

3.4 Mutagenesis analysis of Est2

Two mutants of Est2 (Est2-D18N and Est2-K289E) were designed to explore the mechanism of catalytic and structural discrepancies between Est2 and Est4. The kinetic parameters, substrate specificity, optimum pH and temperature as well as the thermostability of mutants were measured. The mutants Est2-D18N and Est2-K289E showed similar substrate specificity as well as optimum pH and temperature to the wild-type enzyme (**Fig. 3a, 3b & 3c**). Compared with the wild-type enzyme, mutant Est2-D18N had a reduction in both *K*cat and substrate affinity of *p*-NP hexanoate by more than 2.0-fold (**Table 3**). In addition, the thermostability of the mutant Est2-D18N was significantly reduced compared with that of wild-type Est2. The mutant Est2-D18N completely lost activity after incubation at 40°C for one hour (**Fig. 3d**). Mutant Est2-K289E exhibited little deviation from the *K*cat and the *K*m of wild-type Est2. The thermostability and surface potential of Est2-K289E were more similar to those of Est4 than Est2.

4 Discussion

Two novel esterases, Est2 and Est4, which shared 96% amino acid sequence identity, were expressed and characterized in this study. The two enzymes exhibited similar catalytic features, including substrate

specificity, optimum pH and temperature, as well as global structure (**Fig. 3 and Fig. 4**). A notable discrepancy in their catalytic feature is their thermostability. Est2 can sustain 50°C treatment for one hour, while Est4 completely loses its catalytic capability under the same conditions (**Fig. 3d**). To investigate the structural basis of the different thermostabilities of the enzymes, we attempted to obtain their crystal structures for many times. Unfortunately, crystals did not appear and grow (data not shown). Thus, we constructed and compared structural models of Est2 and Est4. The model comparison results suggested that Est2 and Est4 had different surface potentials of the molecule (**Fig. 5a and 5b**). This might result from the different amino acids of the two enzymes that were located on the surface of the molecules. Among the twelve pairs of different amino acids between Est2 and Est4, 6 pairs contained different electrical potentials and polarities. The 6 amino acids in Est2 were the neutral polar amino acids Gln4, Gly63, Thr180 and Gln187, the negatively charged polar amino acid Asp18, and the positively charged polar amino acid Lys289. In Est4, they are the negatively charged polar amino acids Glu4 and Glu289, the polar amino acid Asn18, the nonpolar amino acids Ala63 and Ile180, and the positively charged polar amino acid Arg187. The amino acid residues at positions 18 and 289 had significant differences in charge between the two enzymes.

To analyze the mechanism of different catalytic features between Est2 and Est4, mutants Est2-D18N and Est2-K289E were induced and expressed. The residue Asp18 was located at the cap domain of Est2. The Lys289 was located at the a9-helix. The mutation of residues Asp18 and Lys289 both changed the surface potential (**Fig. 5c and 5d**) and reduced the thermostability of wild-type Est2 (**Fig. 3d**). In previous studies, the surface potential was considered to be crucial for the salinity tolerance of esterase that was isolated from halophilic archaea(Muller-Santos et al. 2009). In this study, the thermostability of mutants was reduced in accordance with the changes in the surface potential of Est2, indicating that the surface potential might also determine the thermostability of the enzyme. The thermostability and surface potential of mutant Est2-K289E were similar to those of Est4 (**Fig. 3d, and Fig. 5b & 5d**), indicating that residue Lys289 may play a key role in determining the discrepancy of surface potential and thermostability between Est2 and Est4.

The cap domain has been reported to have an effect on the substrate specificity and catalytic activity of enzymes(Holmquist 2000). In this study, the mutation of residue Asp18 located at the cap domain dramatically reduced the thermostability (**Fig. 3d**) and catalytic activity of Est2 (**Table 3**). An increase in the *K*m value and a decrease in the *k*cat value toward *p*-NP hexanoate were observed (from (55.0±3.0) μM and (352.4±2.9) s^{-1} to (147.2±14.4) μM and (159.1±4.4) s^{-1}, respectively), suggesting that both the capability of substrate binding and the turnover rate of the enzyme–substrate complex to product were decreased (**Table 3**). Decreases in both *k*cat and *K*m values toward the *p*-NP butyrate substrate indicated that the turnover rate of the enzyme–substrate complex decreased while the substrate affinity of *p*-NP butyrate was increased by the mutation. Compared with mutant Est2-K289E, mutant Est2-D18N had dramatic impacts on the thermostability and catalytic activity of the enzyme. This might result from changes in both the surface potential and mobility of the cap domain attributed to the mutation of Asp18 to Asn18.

5 Conclusions

In summary, two novel family IV esterases, Est2 and Est4, were expressed and characterized from a deep-sea sediment metagenomic library. The two esterases showed high amino acid sequence identity (96%) and shared most catalytic features except thermostability. The structural modeling and mutagenesis of Est2 and Est4 provided insight into the determinants of thermostability. Moreover, residue Asp18 in the cap domain of Est2 showed a marked impact on the thermostability and catalytic activity of Est2. Residue Lys289 determined the differences between Est2 and Est4 in the surface potential and thermostability. The characterization and mechanistic analysis of these enzymes should provide a basis for further exploration of their potential biotechnological applications.

Declarations

Funding

This research was supported by China Ocean Mineral Resources R & D Association (COMRA) Special Foundation under contract No. DY135-B2-10, the Scientific Research Fund of the Second Institute of Oceanography, MNR under contract No. JT1702 and the National Natural Science Foundation of China under contract No. 41876182.

Conflict of interest

The authors declare no conflict of interest.

Ethical approval

This study does not include any experimental procedure performed on humans or animals.

Acknowledgements

The 3D structures of Est2 and Est4 were modeled on the free online server of I-TASSER server (https://zhanglab.ccmb.med.umich.edu).

References

1. Arpigny JL, Jaeger K-E (1999) Bacterial lipolytic enzymes: classification and properties. Biochem J 343:177–183. https://doi.org/10.1042/0264-6021:3430177
2. Bornscheuer UT (2002) Microbial carboxyl esterases: classification, properties and application in biocatalysis. FEMS Microbiol Rev 26:73–81. https://doi.org/10.1111/j.1574-6976.2002.tb00599.x
3. Fu C, Hu Y, Xie F et al (2011) Molecular cloning and characterization of a new cold-active esterase from a deep-sea metagenomic library. Appl Microbiol Biotechnol 90(3):961–970. https://doi.org/10.1007/s00253-010-3079-0

4. Holmquist M (2000) Alpha/Beta-Hydrolase Fold Enzymes: Structures, Functions and Mechanisms. Curr Protein Peptide Sci 1(2):209–235. https://doi.org/10.2174/1389203003381405
5. Hu Y, Fu C, Huang Y et al (2010) Novel lipolytic genes from the microbial metagenomic library of the South China Sea marine sediment. FEMS Microbiol Ecol 72(2):228–237. https://doi.org/10.1111/j.1574-6941.2010.00851.x
6. Huo YY, Jian SL, Cheng H, Rong Z, Cui HL, Xu XW (2018) Two novel deep-sea sediment metagenome-derived esterases: residue 199 is the determinant of substrate specificity and preference. Microb Cell Fact 17(1):16. https://doi.org/10.1186/s12934-018-0864-4
7. Jaeger KE, Eggert T (2002) Lipases for biotechnology. Curr Opin Biotechnol 13:390–397. https://doi.org/10.1016/S0958-1669(02)00341-5
8. Jiang X, Xu X, Huo Y et al (2012) Identification and characterization of novel esterases from a deep-sea sediment metagenome. Arch Microbiol 194(3):207–214. https://doi.org/10.1007/s00203-011-0745-2
9. Jin P, Pei X, Du P et al (2012) Overexpression and characterization of a new organic solvent-tolerant esterase derived from soil metagenomic DNA. Bioresour Technol 116:234–240. https://doi.org/10.1016/j.biortech.2011.10.087
10. Kumar S, Stecher G, Tamura K (2016) MEGA7: Molecular Evolutionary Genetics Analysis version 7.0 for bigger datasets. Mol Biol Evol 33:1870–1874. https://doi.org/10.1093/molbev/msw054
11. Larkin MA, Blackshields G, Brown NP et al (2007) Clustal W and Clustal X version 2.0. Bioinformatics 23(21):2947–2948. https://doi.org/10.1093/bioinformatics/btm404
12. Lee SW, Won K, Lim HK, Kim JC, Choi GJ, Cho KY (2004) Screening for novel lipolytic enzymes from uncultured soil microorganisms. Appl Microbiol Biotechnol 65(6):720–726. https://doi.org/10.1007/s00253-004-1722-3
13. Li J, Zhang K, Han W (2010) Cloning and biochemical characterization of a novel lipolytic gene from activated sludge metagenome, and its gene product. Microb Cell Fact 9(83):1–9. https://doi.org/10.1186/1475-2859-9-83
14. Li PY, Chen XL, Ji P et al (2015) Interdomain hydrophobic interactions modulate the thermostability of microbial esterases from the hormone-sensitive lipase family. J Biol Chem 290(17):11188–11198. https://doi.org/10.1074/jbc.M115.646182
15. Mandrich L, Menchise V, Alterio V et al (2008) Functional and structural features of the oxyanion hole in a thermophilic esterase from Alicyclobacillus acidocaldarius. Proteins 71(4):1721–1731. https://doi.org/10.1002/prot.21877
16. Mandrich L, Merone L, Pezzullo M et al (2005) Role of the N terminus in enzyme activity, stability and specificity in thermophilic esterases belonging to the HSL family. J Mol Biol 345(3):501–512. https://doi.org/10.1016/j.jmb.2004.10.035
17. Muller-Santos M, de Souza EM, Pedrosa Fde O et al (2009) First evidence for the salt-dependent folding and activity of an esterase from the halophilic archaea *Haloarcula marismortui*. BBA-Mol Cell Biol L 1791(8):719–729. https://doi.org/10.1016/j.bbalip.2009.03.006

18. Ollis DL, Cheah E, Cygler M et al (1992) The a/β hydrolase fold. Protein Eng Des Sel 5(3):197–211. https://doi.org/10.1093/protein/5.3.197
19. Park HJ, Jeon JH, Kang SG, Lee JH, Lee SA, Kim HK (2007) Functional expression and refolding of new alkaline esterase, EM2L8 from deep-sea sediment metagenome. Protein Expr Purif 52(2):340–347. https://doi.org/10.1016/j.pep.2006.10.010
20. Rappe MS, Giovannoni SJ (2003) The uncultured microbial majority. Annu Rev Microbiol 57:369–394. https://doi.org/10.1146/annurev.micro.57.030502.090759
21. Robert X, Gouet P (2014) Deciphering key features in protein structures with the new ENDscript server. Nucleic Acids Res 42(W1):W320–W324. https://doi.org/10.1093/nar/gku316
22. Roy A, Kucukural A, Zhang Y (2010) I-TASSER: a unified platform for automated protein structure and function prediction. Nat Protoc 5(4):725–738. https://doi.org/10.1038/nprot.2010.5
23. Samoylova YV, Sorokina KN, Romanenko MV, Parmon VN (2018) Cloning, expression and characterization of the esterase estUT1 from *Ureibacillus thermosphaericus* which belongs to a new lipase family XVIII. Extremophiles 22(2):271–285. https://doi.org/10.1007/s00792-018-0996-9
24. Zhang A, Zhao R, Jin P et al (2013) Discovery of a novel esterase subfamily sharing an identified arm sequence (ArmEst) by gene-specific metagenomic PCR. Biotechnol Lett 35(11):1937–1944. https://doi.org/10.1007/s10529-013-1293-4
25. Zhang H, Li F, Chen H et al (2015) Cloning, expression and characterization of a novel esterase from a South China Sea sediment metagenome. Chin J Oceanol Limnol 33(4):819–827. https://doi.org/10.1007/s00343-015-4170-2
26. Zhu Y, Li J, Cai H, Ni H, Xiao A, Hou L (2013) Characterization of a new and thermostable esterase from a metagenomic library. Microbiol Res 168(9):589–597. https://doi.org/10.1016/j.micres.2013.04.004

Tables

Table 1 Primers used in this study

Esterase	Primer	Nucleotide sequence
Est2	Forward	5'-ATTCCATATGGCCAGCCAGCAACTTC-3'
	Reverse	5'-ACCCAAGCTTATCGGGCTGACGTCTTC-3'
Est4	Forward	5'-ATTCCATATGCCCAGCGAGCAGCTTC-3'
	Reverse	5'-TCCCAAGCTTATCGGGCTGACGTCTTC-3'
Est2-D18N	Forward	5'-ATCAGCTCCCGCCCGAACCTGCGCGGT-3'
	Reverse	5'-TCGGGCGGGAGCTGATCGCCTGGAT-3'
Est2-K289E	Forward	5'-ATCGACCGCATCGGCGAGTTCATGCG-3'
	Reverse	5'-CGCCGATGCGGTCGATAGCCTGCTGG-3'

Note: *Nde*I and *Hin*dIII restriction sites and modified codons are underlined.

Table 2 Esterases most similar to Est2 and Est4 in the GenBank nr database

Esterase	Accession number	Source	Identity/%		Reference
			Est2	Est4	
FLS10	ACL67845	Deep-sea sediment metagenome	78.1	77.1	(Hu et al. 2010)
FLS15	ACL67849	Deep-sea sediment metagenome	77.8	76.8	(Hu et al. 2010)
ScsEst01	AIN40937	Deep-sea sediment metagenome	77.8	77.1	(Zhang et al. 2015)
EstMY09-1	ADM67447	Activated sludge metagenome	72.8	73.4	(Li et al. 2010)
EstMY09-2	ADM67446	Activated sludge metagenome	69.0	69.7	(Li et al. 2010)
Est10	ADA70030	Deep-sea sediment metagenome	68.4	68.0	(Fu et al. 2011)
ELP11B	AAS77236	Soil metagenome	67.4	65.6	(Lee et al. 2004)
ELP45	AAS77233	Soil metagenome	67.0	65.3	(Lee et al. 2004)
ArmEst1	AGF91877	Soil metagenome	66.4	64.4	(Zhang et al. 2013)
EstC23	AFC77925	Soil metagenome	66.4	64.4	(Jin et al. 2012)

Table 3 Kinetic parameters of Est2, Est4 and Est2 mutants

Enzyme	Substrates	V_{max}/μmol·mg^{-1}·min^{-1}	K_m/μM	Kcat/s^{-1}	(Kcat/K_m) /s^{-1}·μM^{-1}
Est2	*p*-Nitrophenol butyrate	791.5±18.7	386.3±24.6	427.8±10.1	1.11
	p-Nitrophenyl hexanoate	652.0±5.3	55.0±3.0	352.4±2.9	6.41
Est4	*p*-Nitrophenol butyrate	620.2±16.4	356.9±26.4	335.9±8.9	0.94
	p-Nitrophenyl hexanoate	605.6±5.9	55.0±3.2	328.0±3.2	5.96
Est2-D18N	*p*-Nitrophenol butyrate	261.8±4.8	359.8±17.9	141.5±2.6	0.39
	p-Nitrophenyl hexanoate	294.3±8.2	147.2±14.4	159.1±4.4	1.08
Est2-K289E	*p*-Nitrophenol butyrate	734.7±25.1	414.2±36.2	397.1±13.6	0.96
	p-Nitrophenyl hexanoate	561.9±4.4	74.1±3.4	303.7±2.4	4.10

Table 4 Effects of various metal ions and chelating agents on the activity of Est2 and Est4

Metals and chelating agent /10 mM	Relative activity/%	
	Est2	Est4
Control	100.0±2.0	99.4±0.5
Ba^{2+*}	75.9±1.2	94.3±0.9
Ca^{2+*}	42.5±1.0	66.7±1.7
Co^{2+*}	84.4±1.2	64.3±0.3
Cu^{2+}	0	0
Mg^{2+}	86.3±0.3	82.6±2.5
Mn^{2+}	19.0±0.6	31.5±1.9
Ni^{2+*}	6.2±0.8	21.1±0.4
Sr^{2+*}	79.4±0.6	91.7±0.7
Zn^{2+*}	16.6±0.4	21.2±0.3
EDTA*	116.2±2.2	104.4±0.6

Note: The activity observed without metal ions or chelating agents was taken as 100%. * $p < 0.05$, representing a significant difference between Est2 and Est4 (Student's t test).

Table 5 Effects of various organic solvents and detergents on the activity of Est2 and Est4

Solvent types/15%	Relative activity/%		Detergents/1%	Relative activity/%	
	Est2	Est4		Est2	Est4
Control	100.0±1.4	99.9±1.8	Control	100.0±1.4	99.9±1.8
Acetone*	0	4.2±0.5	SDS	0	0
Acetonitrile*	37.3±1.7	71.9±6.0	Triton X-100*	45.2±1.0	57.0±0.3
Alcohol*	3.3±0.5	38.7±3.3	Tween 20*	139.8±0.4	86.9±2.0
DMF*	7.8±0.3	8.5±0.2	Tween 80*	34.6±0.7	12.9±0.6
DMSO*	69.4±1.0	80.5±1.4			
Glycerol*	86.2±1.9	75.2±0.6			
Isopropanol*	24.3±0.5	47.0±3.3			
Methanol*	43.9±0.3	70.7±4.1			

Note: The activity observed without organic solvent or detergent was taken as 100%. * $p < 0.05$, representing a significant difference between Est2 and Est4 (Student's t test).

Figures

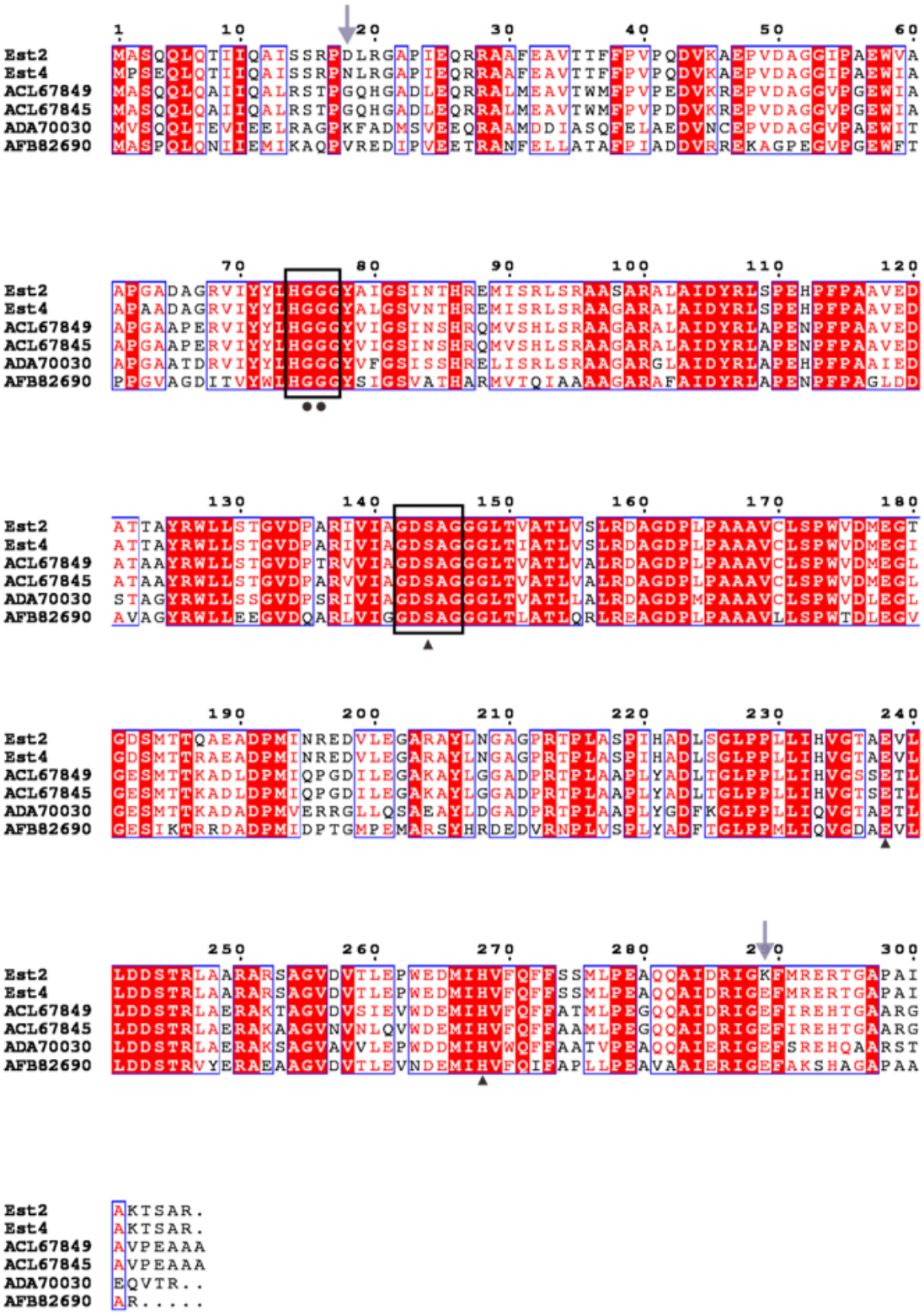

Figure 1

Amino acid sequence alignment of Est2 and Est4 with related lipolytic enzymes. Sequence alignment was performed using the ClustalX and ESPript programs. Identical and similar residues among groups are indicated in white text on a red background and in red text on a white background, respectively. Solid circles indicate the locations of the residues involved in the oxyanion hole (glycine (G)). The catalytic active site residues (serine (S), glutamic acid (E), and histidine (H)) are indicated by triangles. The

conserved HGGG and GDSAG motifs, in which the oxyanion hole and catalytic triad are located, respectively, are outlined with boxes. The purple arrows indicate the locations of residues Asp18 and Lys289 of Est2.

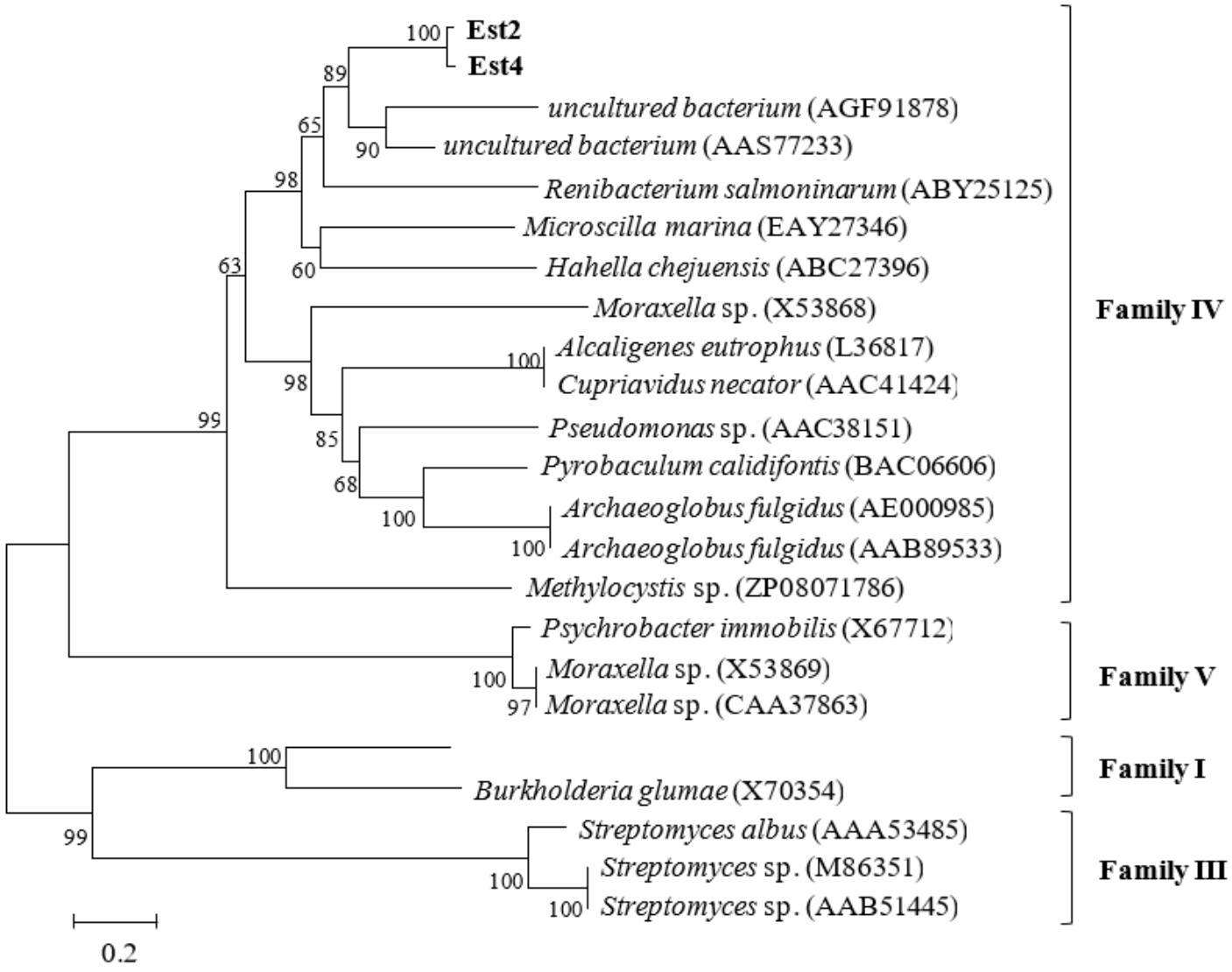

Figure 2

Neighbor-joining phylogenetic tree based on amino acid sequences of Est2 and Est4. Sequence alignment was performed using ClustalX. The phylogenetic tree was constructed by MEGA software. Bootstrap values were based on 1 000 replicates, and values higher than 50% are shown in the tree. The scale bar measured the number of amino acid substitutions per site.

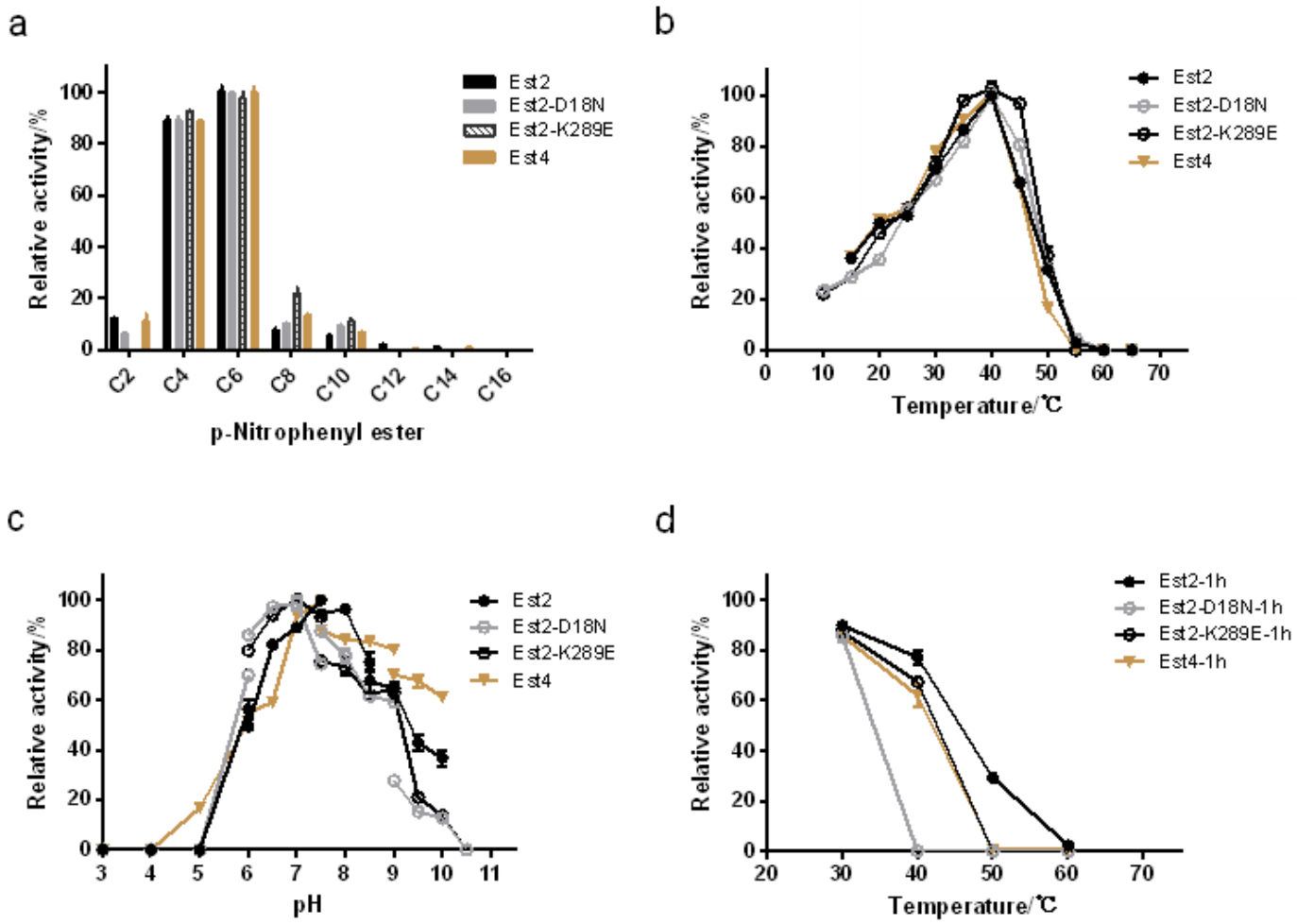

Figure 3

Characterization of Est2, Est4, and two Est2 mutants. a. Substrate specificity was determined using the p-NP esters, including p-NP acetate (C2), p-NP butyrate (C4), p-NP hexanoate (C6), p-NP caprylate (C8), p-NP decanoate (C10), p-NP laurate (C12), p-NP myristate (C14), and p-NP palmitate (C16). All of the tests were performed at 40°C and pH 7.0. b. The effects of pH on the activity were determined by using p-NP hexanoate as the substrate at 40°C in different buffers: 100 mM citrate buffer (pH 3.0–6.0), 100 mM phosphate buffer (pH 6.0–7.5), 100 mM tricine buffer (pH 7.5–9.0), and 50 mM CHES buffer (pH 9.0–10.0). c. The effects of temperature on the activity were determined at various temperatures at pH 7.0 using p-NP hexanoate as the substrate. The highest activity was taken as 100% d. Thermostability of Est2, Est4 and two mutants of Est2 at different temperatures. The relative activities of Est2 and Est4 are based on their initial activities, which are 100%. Data are presented as the mean ± SD (n = 3).

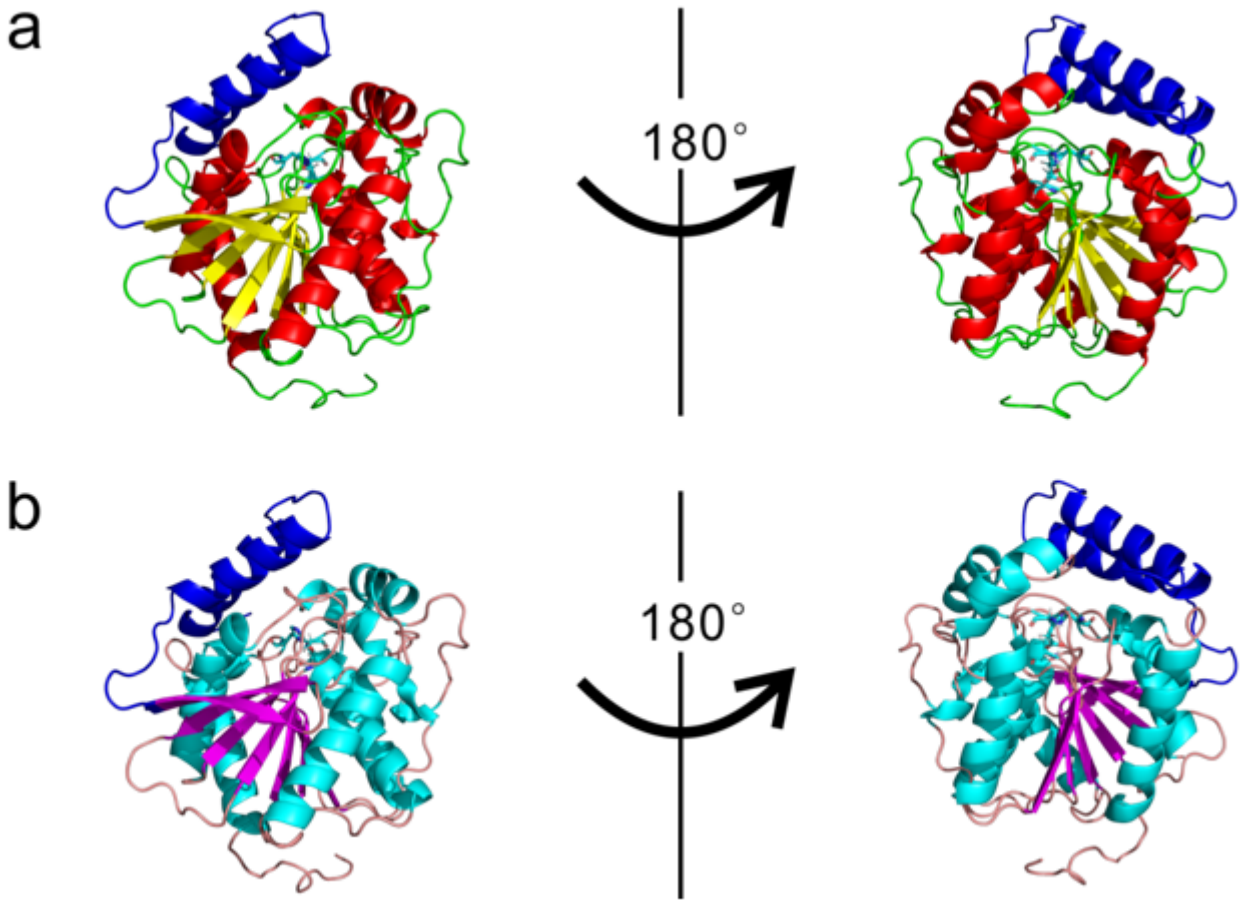

Figure 4

The 3D structural models of Est2 (a) and Est4 (b). Models were constructed by I-TASSER server. The catalytic domains of Est2 are shown in red and yellow, while the catalytic domains of Est4 are shown in sky blue and purple. The cap domains of both are shown in dark blue. The catalytic triad residues are indicated as stick models.

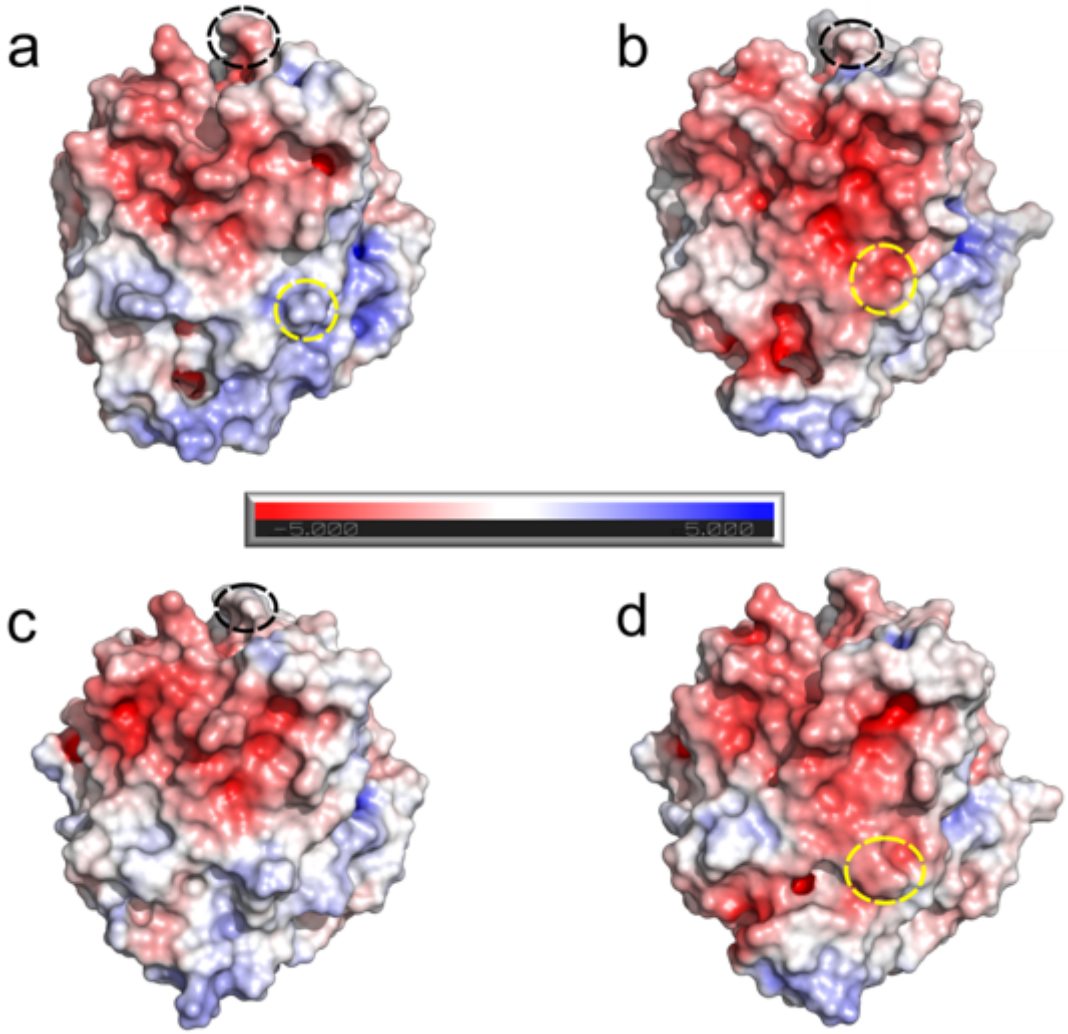

Figure 5

Surface electrostatic potentials of Est2 (a), Est4 (b), Est2-D18N (c) and Est2-K289E (d). Positive and negative electrostatic potentials are indicated by blue and red, respectively. The surface electrostatic potential was obtained by PyMoL and the APBS plugin. The locations of residues Asp18 in Est2 and Asn18 in Est4 are shown in black dashed circles. The locations of residues Lys289 in Est2 and Glu289 in Est4 are shown in yellow dashed circles.